# Gold Mineralization at the Maletoyvayam Deposit (Koryak Highland, Russia) and Physicochemical Conditions of Its Formation

**Evgeny G. Sidorov [1], Andrey A. Borovikov [2], Nadezhda D. Tolstykh [2,3,*], Daria S. Bukhanova [1], Galina A. Palyanova [2,3] and Valery M. Chubarov [1]**

[1] Institute of Volcanology and Seismology, Far East Branch of Russian Academy of Sciences, Piipa Blvd., 9, Petropavlovsk-Kamchatsky 683006, Russia; eg_sidorov@mail.ru (E.G.S.); dasha-snejinka@yandex.ru (D.S.B.); camebax@gmail.com (V.M.C.)

[2] Sobolev Institute of Geology and Mineralogy, Siberian Branch of Russian Academy of Sciences, Koptyuga Ave., 3, Novosibirsk 630090, Russia; borovikov.57@mail.ru (A.A.B.); palyan@igm.nsc.ru (G.A.P.)

[3] Department of Geology and Geophysics, Novosibirsk State University, Pirogova Ave., 2, Novosibirsk 630090, Russia

*** Correspondence: tolst@igm.nsc.ru

check for updates

**Abstract:** Microthermometry study of fluid inclusions in quartz veins of the Maletoyvayam deposit (Koryak Highland, Russia) was carried out. This epithermal gold deposit contains unique Au compounds including maletoyvayamite, which has not been reported anywhere else. Two paragenetic mineral associations (pyrite-quartz and maletoyvayamite-quartz) with quartz of different generations corresponding to different pulses were also described. Only early generations of quartz ($Q^1$) include ore minerals: pyrite for the first mineral assemblage, and in Au-bearing minerals, sulfosalts, bismuthinite, and others—for the second assemblage. A study on fluid inclusions in quartz showed a salinity (mainly NaCl + KCl) range from 0.2 to 4.3 wt.% NaCl eq., increasing from the first mineral association to the second due to boiling fluids. The obtained temperature variations for quartz crystallization were 295–135 °C, the fluid pressure ranged from 79 to 4 bar. On the other hand, the range of conditions obtained for the gold productive ore association is more narrow: salinity of the fluid inclusions is 4.3 wt.% NaCl eq., the temperatures vary from 255 °C to 245 °C, and the pressure from 39 to 32 bar. These physicochemical characteristics of the Maletoyvayam ore deposit greatly coincide with other HS-type epithermal deposits; however, within the Central Kamchatka Volcanic Belt it is so far the only deposit of this type reported.

**Keywords:** Central Kamchatka Volcanic Belt; HS epithermal deposit; maletoyvayamite-quartz association; fluid inclusions; gold

## 1. Introduction

The term "epithermal" was defined by W. Lindgren [1] to include a broad range of tellurides, antimonides or selenides of Au, Ag and base metals deposits which he estimated to be formed from aqueous fluids at low temperatures (less than 200 °C) and moderate pressures. It is, however, now generally accepted that mainly magmatic fluids at slightly higher temperatures (200–300 °C) and pressures of less than a few hundred bars participate in the formation of these type of deposits. Nevertheless, the term "epithermal" is still widespread [2].

Taylor, Hedenquist and coauthors [3,4] consider that an epithermal Au deposit consists of three subtypes: high sulfidation (HS), intermediate sulfidation (IS), and low sulfidation (LS), each represented by characteristic alteration mineral assemblages, occurrences, textures, and characteristic suites of

associated geochemical elements. The term HS (high sulfidation) is now widely used [5], and combines many other previously described types: enargite–gold [6], Goldfield-type [7,8], high-sulfur [9,10], quartz-alunite [11] and alunite–kaolinite [12] which were assigned to a group of epithermal deposits based on their mineralogical and geochemical features. HS type deposits are characterized by the presence of diagnostic minerals of high sulfidation conditions (e.g., enargite), acidic hydrothermal conditions (e.g., alunite, kaolinite) and relatively oxidized conditions of sulfur ($SO_2$-rich) in the hydrothermal system. HS deposits are associated with some types of hydrothermal systems due to influence of a deep magma chamber [13] and also with andesitic volcanoes in which surface manifestations include high-temperature fumaroles and acid sulfate-chloride hot springs. In contrast, LS deposits of reduced ($H_2S$-rich) hydrothermal fluids with neutral pH are similar to those found in geothermal systems [13], that exhibit in the surface: sinter-terraces of silica, hot springs and steam-heated acid-sulfate alterations [14].

Within the Kamchatka Peninsula, Au-Ag epithermal deposits are localized in volcanic belts of different ages (Eocene-Oligocene Koryak-West Kamchatka, Oligocene-Quaternary Central Kamchatka, and Pliocene-Quaternary East Kamchatka), extending along the modern subduction trend [15–19]. All of the Au-Ag mines located there (Aginskoe, Asacha, Ametistovoe, Zolotoe, Baran'evskoe, Kungurtsevskoe, Oganchinskoe, Ozernovskoe), as well as most of the known Au-Ag deposits and prospects, fit into the LS epithermal type [19–23]. These deposits are characterized by the presence of quartz, adularia, illite and calcite in Au-Ag-bearing veins.

The Maletoyvayam deposit located in the Central Kamchatka Volcanic Belt (CKVB) is restricted to volcano–tectonic structures within the Vetrovayam volcanic zone situated in the northeastern part of the CKVB (southwestern part of the Koryak Highland) [24,25]. On the contrary to the above mentioned deposits, Maletoyvayam deposit belongs to the HS type category of epithermal deposits [26], which are also known in the Eastern part of Russia (Belaya Gora and Svetloye) [27]. The predominance of andesite and basaltic andesite rocks in the CKVB is a reflection of the mafic composition of its basement. This factor determines the particularity of the metallogeny on this zone, characterized by a wide development of near-surface mineralization of tellurides as subtypes of the main gold-silver deposits [28]. The veins of massive quartz are included in the vuggy silica, and both are Au(Ag)-bearing. The central vuggy silica zones are rimmed along the periphery of the ore field by quartz-alunite-kaolinite association. The Maletoyvayam HS type deposit differs from others known on the Kamchatka Peninsula, which are of the LS type, by a great variety of mineral phases: native gold, chalcogenides of Au and Ag, Cu-sulfosalts with Sb and As, as well as complexes including Au-bearing oxides among which some are considered rare or unique. Contrary to the other deposits of the CKVB, native gold in these ores is not dominant. The study of other styles of gold occurrences in sulfide-telluride-selenide ores and the physicochemical conditions of their formation are of great interest from a mineralogical, genetic and technological point of view [29]. The first results on the mineral composition of Maletoyvayam deposit were obtained recently [26,30–35]. Typical and uncommon minerals of epithermal systems were reported in this deposit: senarmontite ($Sb_2O_3$), tripuhyite ($FeSbO_4$), bismite ($Bi_2O_3$), rooseveltite ($Bi(AsO_4)$), tiemannite (HgSe), antimonselite ($Sb_2Se_3$), Te-,Sb-bearing guanajuatite: ($Bi_2(Se,Te)_3$ and $(Bi,Sb)_2Se_3$), bismuthinite (($Bi_2S_3$) and $(Bi,Sb)_2(S,Se)_3$), unnamed phase (($Sb,Bi,Te,As,Fe)_2O_5$), tellurium (Te,Se). In addition, unique compounds, that had not been previously found in nature, were reported: maletoyvayamite and its S-rich analogue ($Au_3Se_4Te_6$ and $Au_3S_4Te_6$), AuSe and Au(Te,Se); their occurrence is due most likely to specific properties of the hydrothermal solutions. Microthermometric study of these ores had not previously been carried out. Thus, the purpose of this study is to present mineralogical and microthermometric measurement data of this particular type of ore and to show the physicochemical conditions that played an important role in the ore accumulation.

## 2. Regional Geology and Mineralization

The Central Kamchatka Volcanic Belt (Russia) is about 1800 km long, controlled by the Main Kamchatka deep fault, displaying a significant number of gold-silver epithermal deposits [22,28]. The Maletoyvayam deposit is particularly confined to a volcano-tectonic structure (up to 30 km) within the Vetrovayam volcanic zone located in the northeastern region of the Central Kamchatka Volcanic Belt and delimited by the Koryak Highland in the southwestern part [24,25]. This whole structure is controlled by the Vyvensky northeast-striking deep fault and the northwest-striking faults zone [36,37]. Stratified subvolcanic and intrusive formations, as well as Quaternary sediments, are the constituent elements of the ore field (Figure 1).
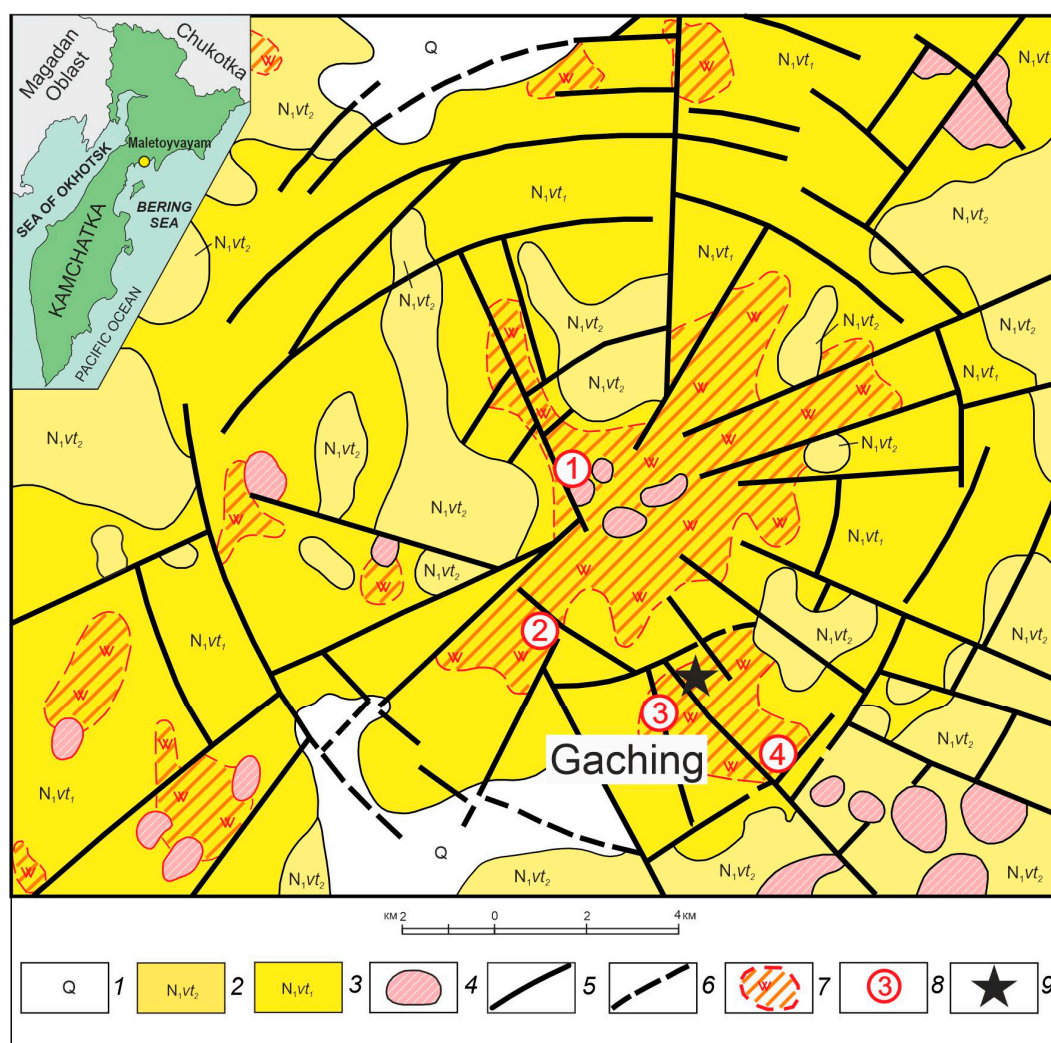


**Figure 1.** Schematic geological map (volcano-tectonic structure) of the Maletoyvayam gold deposit, modified after Stefanov and Schiroky [37]. 1—Quaternary deposits; 2,3—rocks of the upper member (2) and the lower member (3) of the Vetrovayam Formation (Middle-Late Miocene); 4—Vetrovayam volcanic complex (Late Miocene); 5—main faults; 6—faults covered by Quaternary deposits; 7—hydrothermally altered rocks; 8—ore occurrences (numbers in circles): 1—Yubileyny, 2—Yugo-Zapadny, 3—Gaching, 4—Tyulul; 9—Sampling location.

Stratified deposits are represented by effusive, pyroclastic, and tuffaceous-sedimentary rocks of the Vetrovayam Formation (Figure 1), which are divided into two lithostratigraphic members. The lower member ($N_1vt_1$) is composed of tuff and tuff breccia of intermediate to basic composition, andesite, basaltic andesite, and, less often, dacite and felsic tuff. At the base of this member, there are lenses

and interlayers of tuffaceous sandstone, tuff conglomerate, tuff siltstone, and brown coal. The upper member ($N_1vt_2$) of the Vevetrovayam Formation is 10–30 m thick and composed mainly by effusive rocks: andesite and basaltic andesite. Interlayers of basalt, tuff, tuff breccia, and tuff conglomerates of intermediate and mafic composition are less common. The radiometric age for effusive rocks (K/Ar method) is 7–18 Ma [38]. Intrusive subvolcanic bodies and dikes form a single volcanic complex (Vetrovayam), which is represented by diorite, quartz diorite and granodiorite. The age of this complex was determined as Middle-Late Miocene [38]. Volcanic rocks in the area exhibit different degrees of hydrothermal alteration, which are associated with areas of gold mineralization and sulfur deposits explored in 1971 [25,36,38]. The Maletoyvayam deposit includes four areas (ore occurrences) where gold ore reserves have been identified and estimated: Yubileyny, Yugo-Zapadny, Gaching and Tyulul.

Based on the types of mineral assemblages [26], these ore occurrences are associated to a HS epithermal type [4,39,40]. However, they differ among themselves in the degree of oxidation of the primary mineralization. For instance, at the Gaching occurrence, the ores are less oxidized (about 10% sulfate iron and 90% sulfide iron), compared to the Yugo-Zapadny occurrence, where sulfide iron is only 8%. Hence, the primary mineralization at the Gaching ore occurrence is considered to be more preserved and for that reason it was selected and analyzed in the present study.

Maletoyvayam deposit is composed of rocks of the lower member of the Vetrovaym Formation. Vuggy silica was identified in the central part of the ore field, transitioning outwards into quartrz-alunite, quartz-kaolinite, quartz-sericite-kaolinite and then to argillic- and propylitic-altered rocks. Gold was found both in vuggy silica remnants located on the watershed in the Gachingalhovayam river valley (Figure 2a), and in quartz veins. The color in rock samples showing vuggy and massive silica texture is light gray to gray (Figure 2b). In the samples with texture the main mineral phase is quartz—85–90 vol.%; kaolinite—5 vol.%, and alunite—4–5 vol.%; the rest of the minerals correspond to potassium feldspar, barite, anglesite, muscovite, etc.



**Figure 2.** (**a**) Vuggy silica in the Gachingalhovayam river valley, (**b**) Vuggy silica sample with quartz veins, (**c**) fragment of quartz vein containing the maletoyvayamite-quartz association, Gaching ore occurrence.

The dark zones in samples exhibiting vuggy silica texture are due to the presence of an intense dissemination of mainly pyrite, or sulfosalts along with gold mineralization. Au content in samples with vuggy silica texture reaches 8.8 ppm, whereas Ag—47.2 ppm. The white quartz veins also contain a fine-grained dissemination of ore minerals, which is irregularly distributed (Figure 2c). The concentration of Au in quartz veins vary within the range 1.40–144 ppm, and for Ag—147–724 ppm. Other ore elements show concentrations of: Cu—1.38–3.18; As—up to 2; S—up to 2.26; Sb, Se, Te—more than 0.2 (wt.%) [25].

## 3. Samples and Analytical Methods

Quartz veins samples selected for this study are shown in (Table 1). In the first stage, thin polished sections were made from these samples. To determine the phases' transition temperatures in quartz fluid inclusions, cryo- and thermometry methods were used (Linkam THMSG-600 heating-freezing chamber

(Linkam Scientific Instruments, Tadworth Surrey, United Kingdom, https://www.linkam.co.uk/) with a measurement range of −196/+600 °C). The composition of the gas phase and corresponding identification of solid phases in the inclusions were carried out by Raman spectroscopy (JobinYvon "Ramanor U-1000" spectrometer, MillenniaProS2 laser (532 nm), HORIBA JOBIN YVON detector, Novosibirsk, Russia).

**Table 1.** List of samples with their main characteristics

| Sample | Texture | Morphology | Minerals Included in Quartz or Filling Cracks and Cavities |
|--------|---------|------------|-----------------------------------------------------------|
| 3053_a | Filling of cavities | Segregation | Fe-hydroxide, Fe-antimonite/tellurite, sulfosalts, Au-Fe(Sb,As,Te) oxide |
| 3053_b | Filling of cavities | Segregation | Sulfosalts, maletoyvayamite, tellurium |
| 3058_a | Interspersed | Inclusions | Pyrite |
| 3058_b | Interspersed | Inclusions | Pyrite |
| 3058_c | Interspersed | Inclusions | Bismuthinite, maletoyvayamite, Sb(Bi,Te,As,Se) oxide, sulfosalts |

Note. All samples are a vein of white quartz.

The total salt concentrations in fluid inclusions and their corresponding water–salt system were determined using the cryometry method [41,42]. The assessment of the pressure of mineral formation environment was carried out using the published pressure-temperature-composition data for NaCl-$H_2O$ systems. The AqSo_NaCl [43], ISOHOR [44] and FLINCOR [45] software packages were also used to estimate the pressure of mineral formation from microthermometric data obtain in the study of fluid inclusions.

The chemical compositions of the minerals (samples 3053-8_a,d,c) and texture of mineral aggregates were studied at the Analytical Center for multi-elemental and isotope research of the Sobolev Institute of Geology and mineralogy Russian Academy of Sciences (SB RAS) in Novosibirsk, using a LEO-413VP scanning electron microscope (SEM) with the INCA Energy 350 microanalysis system (Oxford Instruments Ltd.) equipped with an energy dispersive spectrometer (EDS) (analysts: Dr. N. Karmanov, M. Khlestov), operated at an accelerating voltage of 20 kV, current intensity 0.4 nA, 50 sec. measuring time, and beam diameter ~1 μm. The following standards were used: pure metals (Ag, Au, Bi, Se, Sb, Fe, Cu), pyrite (S), synthetic HgTe (Te), sperrylite (As). The detection limit was 0.02%. The following X-ray lines were selected: Lα for Ag, Te, As, Sb and Se; Kα for S, Fe, Cu and O; and Mα for Au and Bi. Analytical data for the samples 3053-3 a,b was obtained at the Institute of Volcanology and Seismology of Far Eastern Branch of RAS, using a TescanVega-3 scanning electron microscope equipped with an energy dispersive spectrometer, EMF X-MAX (analyst: V.M. Chubarov), operated at an accelerating voltage of 20 kV, current intensity 3–0.7 nA, 50 sec. measuring time, and beam diameter ~1 μm. The following standards were used: pure metals (Au, Ag, Se, Sb), synthetic $FeS_2$ (Fe), InAs (As), CdTe (Te), $CuSbS_2$ (Sb), $Bi_2S_3$ (Bi), $CuFeS_2$ (S, Cu). The detection limit was 0.1 wt.%. The following X-ray lines were selected: Lα for Ag, Te, As, Sb and Se; Kα for S, Fe, Cu and O; and Mα for Au and Bi.

## 4. Results

### 4.1. Mineralogy of Studied Maletoyvayam Deposit Ores

The studied samples are represented by quartz veins with abundant spotty dissemination of fine grain ore minerals. In some of the ore samples only pyrite is present, whereas Au minerals are completely absent. These samples are considered to be related to early pyrite-quartz assemblage (Figure 3a,b). Other samples contain fine dissemination of Au compounds along with other ore minerals; however, pyrite is absent or only represented as subordinate inclusions within other minerals. These samples are genetically associated to the later gold-bearing assemblage [26], which in the context of our study was named as: the maletoyvayamite-quartz association.
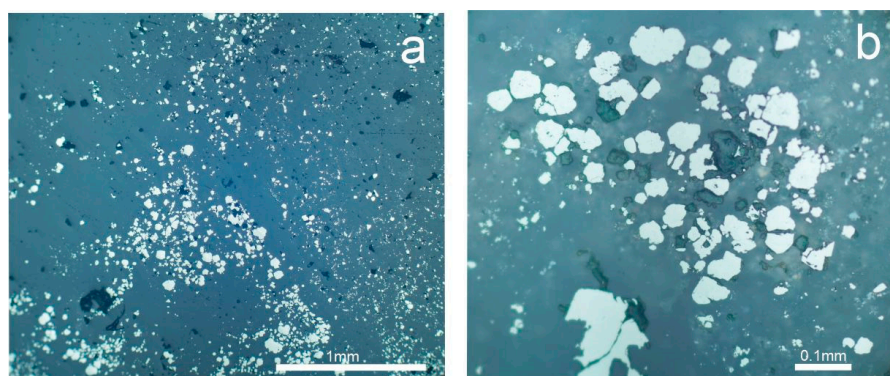
**Figure 3.** Impregnation of pyrite in quartz: irregular (sample 3058-8_a) (**a**) and spotted (**b**) from the pyrite-quartz association (sample 3058-8_b).

The studied ore-bearing samples correspond to quartz veins. The concentrations of noble metals vary depending on the dissemination density within the ore samples: Au from 0.8 to 147 ppm and Ag from 0.5 to 200 ppm. In Au-Ag enriched samples (3053-3), quartz contains very small quartz druses; these cavities are partially or completely filled with a finely dispersed reddish-gray mass, represented by a mixture of iron hydroxides, tellurites and iron antimonates, sulfosalts (Figure 4a), native and secondary (mustard) gold and other rare minerals including unique compounds of Au-sulfoselenotellurides and complex Au-bearing oxides (Figure 4b).
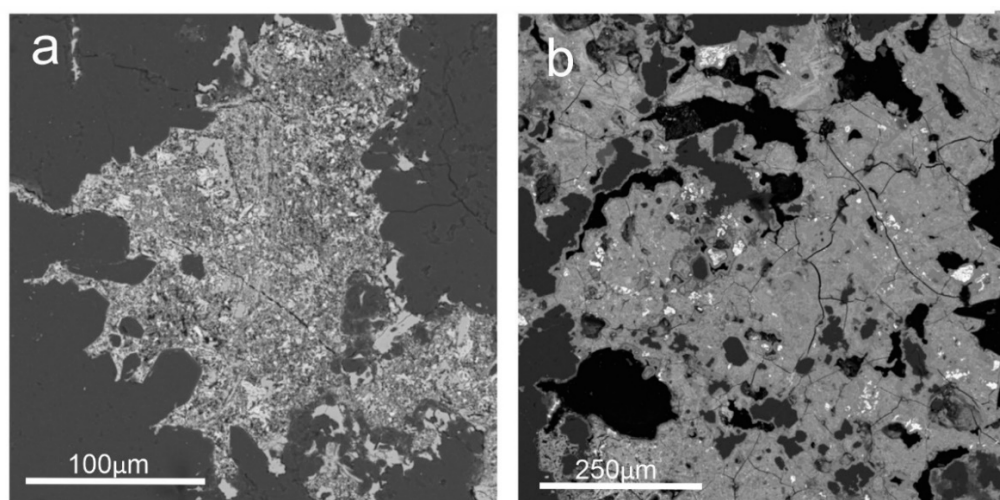


**Figure 4.** SEM image of sample 3053-3_a. The cavities in quartz filled with a finely dispersed mass represented by a mixture of iron hydroxides, tellurites, iron antimonates, and sulfosalts (**a**); and the same masses, but impregnated with complex oxides of Au (Au-Fe-Sb-Te-O compounds) (**b**).

Sulfosalts are widespread in the ore associations of the Maletoyvayam deposit. Two main groups of sulfosalts were identified in the Gaching area: the tetrahedrite-group $Cu_{12}(As,Sb,Te)_4S_{13}$ and enargite-group $Cu_3(As,Sb)S_4$ [33]. In the samples with highest noble metals enrichment, maletoyvayamite occurs as independent grains intergrown with tellurium and sulfosalts. It is often found along cracks or in the intergranular space of quartz (Figure 5a), or confined to the margins of large grains of sulfosalts (Figure 5b).

Au-bearing minerals range in size from a few μm to 80 μm, while sulfosalt grains reach up to 2.5 mm. The sulfosalts are enriched in Se within a range of 5.84–10.42 wt.%. The substitution of Se for S is ubiquitous (Table 2). The presence of selenium in sulfosalts indicates specific conditions for their formation.

**Table 2.** Compositions of ore minerals shown in Figure 5 from the maletoyvayamite-quartz. association (sample 3053-3), wt.%.

| No | S | Cu | As | Se | Sb | Te | Au | Total | Formula |
|---|---|---|---|---|---|---|---|---|---|
| 1 | 21.49 | 42.37 | | 5.84 | 8.46 | 20.75 | | 99.28 | $Cu_{11.82}(Te_{2.86}Sb_{1.22})_{4.08}(S_{11.80}Se_{1.30})_{13.10}$ |
| 2 | 21.43 | 40.28 | 2.30 | 8.76 | 6.40 | 21.38 | | 100.56 | $Cu_{11.05}(Te_{2.92}Sb_{0.92}As_{0.54})_{4.38}(S_{11.65}Se_{1.93})_{13.58}$ |
| 3 | 6.34 | | | 6.24 | | 50.5 | 37.80 | 100.88 | $Au_{2.89}Te_{5.95}(S_{2.97}Se_{1.19})_{4.16}$ |
| 4 | 6.35 | | | 5.60 | | 50.47 | 37.76 | 100.19 | $Au_{2.91}Te_{6.00}(S_{3.01}Se_{1.08})_{4.09}$ |
| 5 | 3.38 | | | 11.03 | | 49.89 | 36.16 | 100.46 | $Au_{2.91}Te_{6.20}(Se_{2.22}S_{1.67})_{3.89}$ |
| 6 | | | | 6.97 | | 92.99 | | 99.95 | $Te_{0.89}Se_{0.11}$ |
| 7 | 25.81 | 42.65 | 6.15 | 7.50 | 17.88 | 0.73 | | 100.72 | $Cu_{4.09}(Sb_{0.89}As_{0.50}Se_{0.48}Te_{0.04})_{1.91}(S_{4.90}Se_{0.10})_{5.00}$ |
| 8 | 20.59 | 42.59 | 1.02 | 7.74 | 12.34 | 15.75 | | 100.03 | $Cu_{11.79}(Te_{2.17}Sb_{1.78}As_{0.24})_{4.19}(S_{11.30}Se_{1.73})_{13.02}$ |
| 9 | | | | 32.8 | | 66.68 | | 99.49 | $Te_{0.56}Se_{0.44}$ |
| 10 | 2.95 | | | 12.15 | | 48.75 | 36.40 | 100.26 | $Au_{2.96}Te_{6.11}(Se_{2.46}S_{1.47})_{3.93}$ |
| 11 | 19.71 | 40.94 | | 9.99 | 8.85 | 20.00 | | 99.49 | $Cu_{11.57}(Te_{2.82}Sb_{1.31})_{4.13}(S_{11.04}Se_{2.27})_{13.31}$ |
| 12 | 26.94 | 45.54 | 16.52 | 10.42 | 2.34 | | | 101.76 | $Cu_{2.97}(As_{0.91}Sb_{0.08})_{0.99}(S_{3.49}Se_{0.55})_{4.04}$ |

Note. 1,2,8,11—goldfieldite $Cu_{12}(Te,Sb)_4(S,Se)_{13}$; 3,4—S-rich analogue of maletoyvayamite $Au_3Te_6(S,Se)_4$; 5,10—maletoyvayamite $Au_3Te_6(Se,S)_4$; 6,9—tellurium; 7—watanabeite $Cu_4(Sb,As)_2(S,Se)_5$; 12—enargite $Cu_3(As,Sb)(S,Se)_4$.
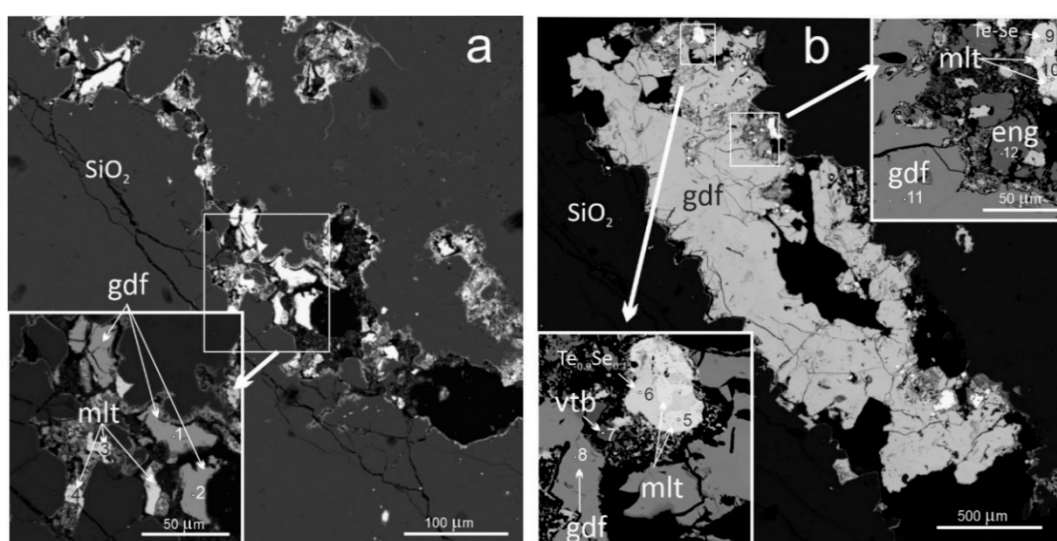


**Figure 5.** SEM image. The maletoyvayamite-quartz association in the sample 3053-3_b, highest enrichment in noble metals (Au is 144 ppm, Ag is 200 ppm); (**a**) ore minerals localized along cracks in the intergranular space of quartz; (**b**) maletoyvayamite confined to the margins of sulfosalts grains; mlt—maletoyvayamite, gdf—goldfieldite, wtb—watanabeite, $Te_{0.9}Se_{0.1}$—Te-Se solid solution. Points with numbers correspond to the analysis numbers in Table 2.

Another sample (3053-8_a,d,c) containing the maletoyvayamite-quartz ore association with concentrations of Au and Ag 1.4 and 12.3 ppm, respectively, contains large bismuthinite inclusions. In addition, sulfosalts of various compositions (tetrahedrite, goldfieldite, enargite, etc.), which are described in [33], are also found in association with bismuthinite (Figure 6a,c,d). Bismuthinite has an unusual composition, since Sb and Te in its structure are substituted for Bi, whereas Se and Te for S (Figure 6a,b; Table 3). Furthermore, it was found that bismuthinite has an S/Se = 2 ratio. Moreover, we suggest the possibility of this mineral phase corresponding to a potentially new mineral $Bi_2S_2Se$. This phase has also been reported from the HS-IS epithermal Perama Hill deposits, in Greece [46]. It is intergrown with the Se-bearing tellurium (Figure 6c). Complex oxides of various oxidation states in primary minerals, including maletoyvayamite, are common in the Maletoyvayam deposit [26,31]. In the analyzed sample, bismuthinite and similar phases are replaced by oxides of Sb, Bi, As, Te and Se in variable proportions; Fe, Cu and occasionally Ag are minor elements. The oxidation state also varies in these compounds from $(Sb,Bi,Te,As,Se)_{0.31}O_{0.69}$ to $(Sb,Bi,Te,As,Se)_{0.24}O_{0.76}$ (Figure 7) depending mainly on the oxygen fugacity: $\log fO_2$ ranging from −29.8 to −27.3; values previously calculated for the ore-bearing mineral association [26].
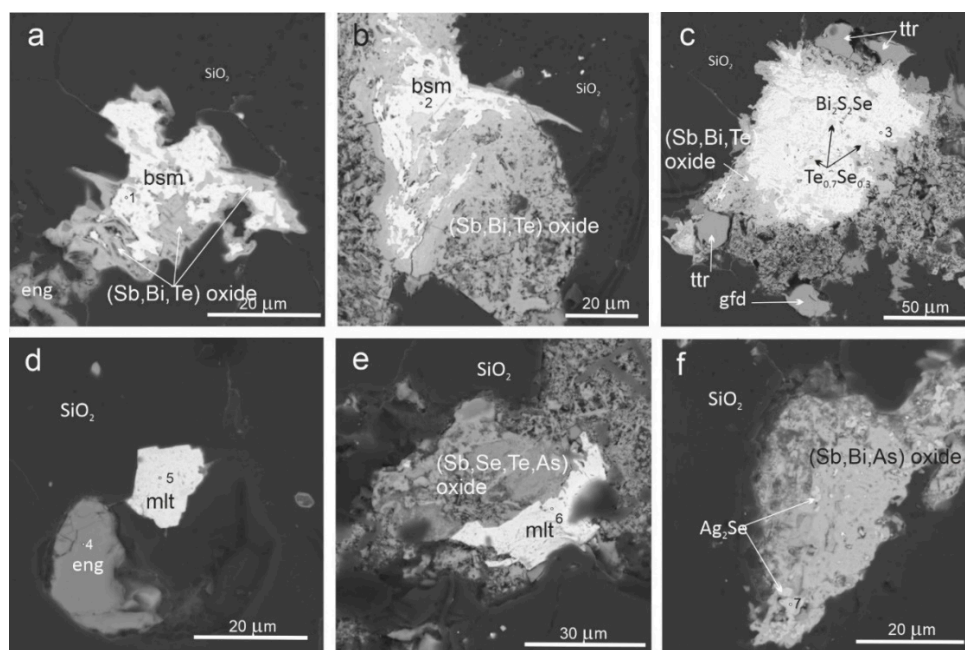
**Figure 6.** SEM image. The maletoyvayamite-quartz association in the sample 3053-8-c (Au is 1.37 ppm and Ag is 12.3 ppm): (**a**) Sb,Te,Se-bearing bismuthinite (bsm) replaced by (Sb,Bi,Te)-oxide in intergrowths with enargite (eng) hosted in quartz; (**b**) bismuthinite replaced by (Sb,Bi,Te)-oxide; (**c**) unnamed phase $Bi_2S_2Se$ with inclusions of Se-rich tellurium ($Te_{0.7}Se_{0.3}$) replaced by (Sb,Bi,Te)-oxide, in intergrowth with tetrahedrite (ttr) and goldfieldite (gfd); (**d**) inclusions of maletoyvayamite (mlt) and enargite in quartz; (**e**) maletoyvayamite in intergrowths with (Sb,Se,Te,As)-oxide; (**f**) grain of (Sb,Bi,As)-oxide containing the naumannite ($Ag_2Se$) inclusions in quartz. Points with numbers correspond to the analysis numbers in Table 3.

**Table 3.** Compositions of ore minerals shown in Figure 6 from the maletoyvayamite-quartz. association (sample 3053-8_c), wt.%.

| No. | Au | Cu | Ag | Bi | Sb | Te | As | Se | S | Total | Formula |
|---|---|---|---|---|---|---|---|---|---|---|---|
| 1 | | | | 62.41 | 8.46 | 2.89 | | 10.89 | 14.16 | 98.81 | $(Bi_{1.54}Sb_{0.36}Te_{0.12})_{2.01}(S_{2.28}Se_{0.71})_{2.99}$ |
| 2 | | | | 65.07 | 5.19 | 3.20 | | 11.36 | 13.45 | 98.27 | $(Bi_{1.65}Sb_{0.23}Te_{0.13})_{2.01}(S_{2.23}Se_{0.76})_{2.99}$ |
| 3 | | | | 72.54 | | | | 14.13 | 11.34 | 98.01 | $Bi_{1.97}S_{2.01}Se_{1.02}$ |
| 4 | | 47.11 | | | | 2.86 | 15.93 | 1.07 | 31.32 | 98.29 | $Cu_{3.01}(As_{0.86}Sb_{0.10})_{0.96}(S_{3.97}Se_{0.06})_{4.03}$ |
| 5 | 35.10 | | | | | 47.38 | | 14.80 | 2.03 | 99.31 | $Au_{2.89}Te_{6.03}(Se_{3.04}S_{1.03})_{4.07}$ |
| 6 | 55.87 | | | | | 47.07 | | 14.67 | 2.14 | 99.75 | $Au_{2.95}Te_{5.97}(Se_{3.01}S_{1.08})_{4.09}$ |
| 7 | | | 71.84 | | | | | 26.49 | | 98.33 | $Ag_{2.00}Se_{1.00}$ |

Note. 1,2—Sb,Te,Se-bearing bismuthinite $(Bi,Sb,Te)_2(S,Se)_3$, 3—unnamed phase, 4 enargite, 5,6—maletoyvayamite, 7—naumannite.
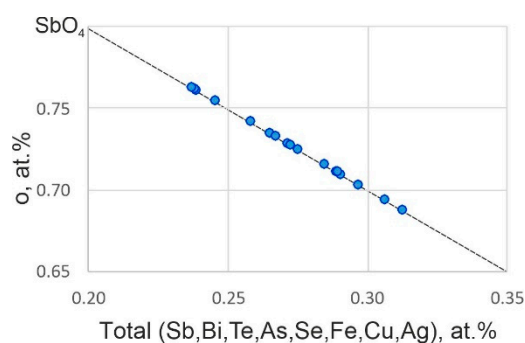


**Figure 7.** Oxygen versus the sum of the rest atoms in complex oxides (iron tellurites and iron antimonates) showing the variations in their composition due to the degree of oxidation of the primary phases.

### 4.2. Quartz Generations and Corresponding Types of Fluid Inclusions

The ore-bearing samples selected to study of fluid inclusions are represented by two main associations: pyrite-quartz and maletoyvayamite-quartz.

#### 4.2.1. Pyrite-Quartz Association

In the studied samples showing this mineral association, there are at least three successively crystallized generations of quartz (Figure 8a). The earliest generation is represented by a grayish to dark gray fine-grained quartz aggregate with abundant dissemination of fine pyrite grains. Subsequent generations of quartz are represented by veins that cut the early pyrite-bearing quartz. In late veinlets, crustified, microdruse, cockade and, less often, collomorphic textures can be observed (Figure 8a). These textures are also representative of mineral associations in other gold-bearing low sulfidation epithermal deposits in the Kamchatka Peninsula [19]. Late quartz veins also contain sporadic pyrite, but very rarely. Separate large grains of quartz in late veinlets are characterized by a zonal structure. The central parts of quartz grains contain single two-phase inclusions with isometric shape (Figure 9b). Growth zones on the periphery of quartz crystals are traced by abundant fluid inclusions with oval vacuoles, elongated perpendicular to the faces of quartz crystals (Figure 9c).
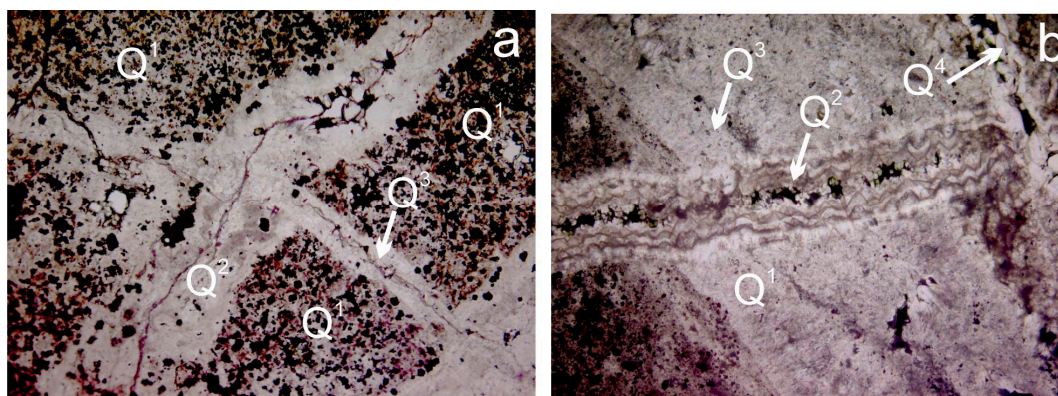


**Figure 8.** Quartz generations. (**a**) pyrite-quartz mineral association: Early quartz ($Q^1$) is presented in association with abundant pyrite grains (black spots) and intersected by veins of quartz ($Q^{2-4}$), containing rare pyrite inclusions; (**b**) maletoyvayamite-quartz mineral association: In this sample, early quartz ($Q^1$) contains inclusions of bismuthinite and maletoyvayamite. This quartz generation is intersected by late quartz veins ($Q^{2-4}$).
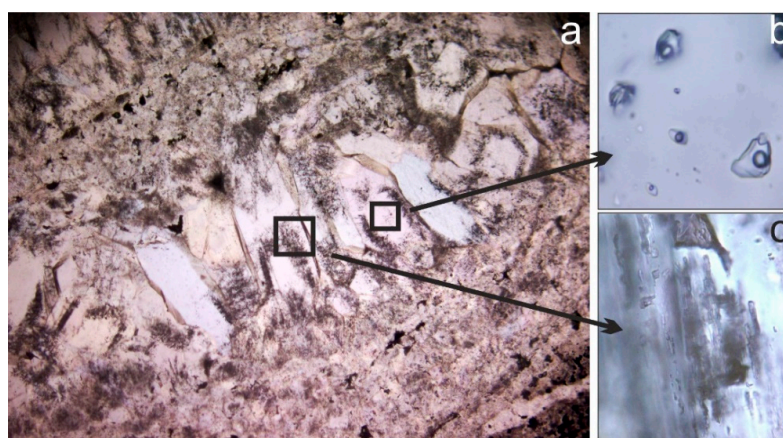


**Figure 9.** (**a**) quartz exhibiting zoning pattern with crustified texture from a pyrite-quartz association; (**b**) a group of isolated two-phase inclusions in the center part of the quartz crystal, (**c**) two-phase inclusions with elongated shape trace the growth zone at the periphery of the quartz crystal.

Crystallization of some quartz generations with different textures occurred close in time or almost simultaneously, since smooth transitions are often observed among them. It is likely that several hydrothermal pulses at very short time intervals were consistently segregated during the formation of ores. Thus, different quartz generations represent the observed textural varieties as a result of these rhythmic pulses. On this subject, when presenting the results on fluid inclusions, showed by textural features, we will divide the quartz in the pyrite-quartz association into only two generations—the early fine-grained generation with abundant dissemination of pyrite and the late one, represented by veinlets cutting the first one.

### 4.2.2. Maletoyvayamite–Quartz Association

Quartz associated with this mineral assemblage is similar to those of the pyrite-quartz association in respect to the textural and structural features, as well as in the distribution of fluid inclusions. Quartz displaying crustified texture also contain inclusions of ore minerals. Pyrite in the studied sample is represented by single small crystals whereas Au minerals (maletoyvayamite) are the most abundant (Figure 6 d,e); among Ag minerals, naumannite $Ag_2Se$ and hessite $Ag_2Te$ occur in association (Figure 6f). The quartz of the maletoyvayamite-quartz association, as in the pyrite-quartz association, also contains two types of fluid inclusions (Figure 10a,b) with the characteristic that they belong to the primary phase, and less often to the pseudo-secondary phase according to [47,48]. The first type is represented by two-phase inclusions close to isometric, containing a gas bubble and liquid in vol. ratios 1/10–1/12, which does not exceed 10 μm in size (Figure 10c). The second type is represented by two-phases, which are close to the faces of the quartz crystal and delimitate its growth zones. They have an elongated or tubular shape of up to 30 μm in length and 5–10 μm in cross-section (Figure 10d), and as a rule, they are associated with single-phase vapor inclusions, also elongated with channel-shaped, of up to 50 μm in length.
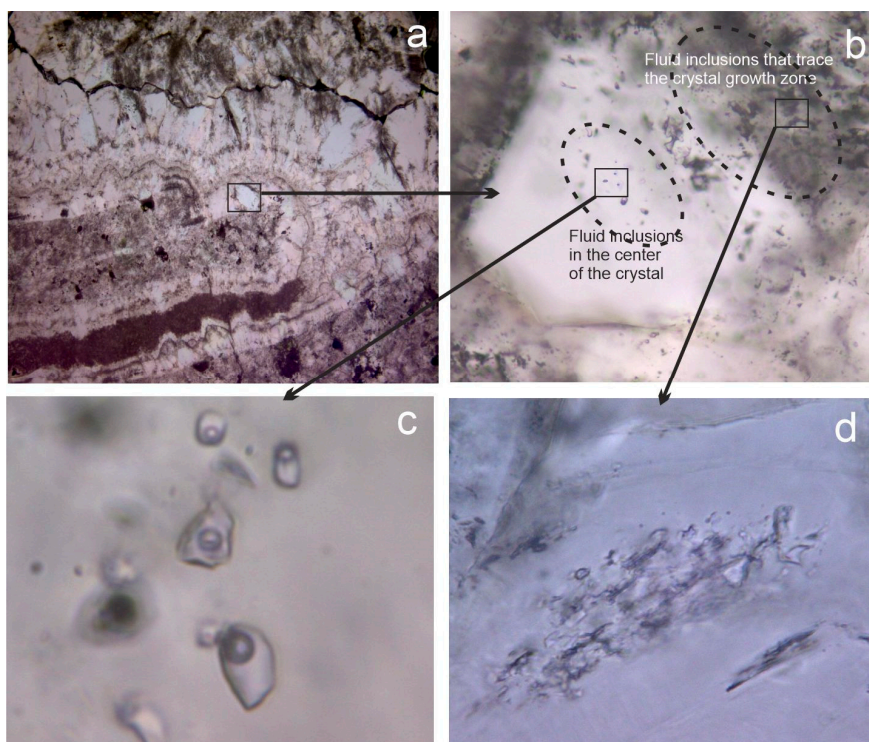


**Figure 10.** (**a**) quartz exhibiting zonation texture from a maletoyvayamite-quartz association; (**b**) group of isolated fluid inclusions in the central part of the quartz crystal and elongated shape of inclusions at the periphery of the crystal; close-up showing the representative shape and details of the inclusions in the center of quartz crystals (**c**) and in the growth zones (**d**).

The origin of elongated fluid inclusions is related with the repulsion of mineral particles by the growing face of the crystal, or with the processes of dissolution of quartz and subsequent healing of the formed tunnel-like hollows [47]. The presence of single-phase vapor inclusions seems to be due to boiling processes of the mineral-forming fluid. Judging by the significant elongation of the vacuoles of fluid inclusions located perpendicular to the faces of the quartz crystal, the boiling process is suggested to be quite long [47].

### 4.3. Results of the Fluid Inclusions Microthermometry

The results of fluid inclusions study from different types of quartz veins associations make it possible to characterize the main physicochemical parameters related to their formation. Table 4 summarizes these main parameters for two types of quartz from the different associations discussed before.

**Table 4.** Results of fluid inclusions microthermometry in quartz from early and late generations.

| Quartz Generation | T °C Homogenization, (n *) | T °C Eutectic | T °C Ice Melting | NaCl, wt.% | KCl, wt.% | Total Salinity, wt.% | Pressure **, Bar |
|---|---|---|---|---|---|---|---|
| **Pyrite-Quartz Association** | | | | | | | |
| Early ($Q^1$) | 290–288 (5) | −25 (−38–−35) | −0.5–−0.4 | 0.6 | 0.3 | 0.9 | 70–68 |
| | 270–260 (6) | −24–−23 | −0.6–−0.4 | 0.6 | 0.3 | 0.9 | 50–43 |
| | 295 (2) | 25 (−38–−35) | −0.5–−0.4 | 0.6 | 0.3 | 0.9 | 76 |
| | 245 (4) | −24.5 | −0.5 | 0.6 | 0.3 | 0.9 | 32 |
| | 264–268 (3) | −26–−25 | −2 | 2.5 | 0.8 | 3.3 | 49 |
| Late ($Q^{2–4}$) | 260–240 (4) | −38 | −0.1 | 0.1 | 0.1 | 0.2 | 43 |
| | 200 (2) | −38–−35 | −0.1 | 0.1 | 0.1 | 0.2 | 13 |
| **Maletoyvayamite-Quartz Association** | | | | | | | |
| Early ($Q^1$) | 255–245 (4) | −38–−35 | −2.5–−2 | 3.3 | 1.0 | 4.3 | 39–32 |
| | 250–245 (2) | −38–−35 | −2.4–−2.2 | 3.3 | 1.0 | 4.3 | 36–32 |
| Late ($Q^{2–4}$) | 228–210 (6) | −38 | −0.7–−0.5 | 1.0 | 0.5 | 1.5 | 23–16 |
| | 220–135 (3) | −38 | −0.6–−0.3 | 0.9 | 0.3 | 1.2 | 20–4 |

Note. * Number of inclusions; ** pressure value calculated for the concentration of solutions (wt.%) to NaCl eq.

#### 4.3.1. Pyrite-Quartz Association

Two-phase water–salt inclusions from early quartz are homogenized at temperatures ranging from 290 to 260 °C. Ice is formed in these inclusion solutions when they are cooled, and melts again when heated at a temperature range from −2 to −0.4 °C. The first melting of ice is observed in a temperature range from −38 to −35 °C, although intense, ice melting and the appearance of liquid in is recorded in the range from −26 to −23 °C. In small inclusions, the first melting is distinguished in the same temperature interval (from −26 to −23 °C), which is close to the melting temperature of the eutectic $NaCl + KCl + H_2O$ water–salt system (−23.5 °C). This may indicate that the main salt components in the inclusions are probably NaCl and KCl with a diminutive admixture of other soluble salts, which somewhat lower the eutectic of the solutions. One of such impurities may correspond to $K_2CO_3$, since the melting temperatures of eutectics in the water–salt systems $Na_2CO_3 + K_2CO_3 + H_2O$ and $K_2CO_3 + H_2O$ correspond to −37 and −36.4 °C [48], that also coincides with a temperature interval of the ice first melting in large inclusions −38–35 °C.

According to the method used by Borisenko [41] it was revealed that the concentrations of Na and K chlorides prevailing in the composition of solutions in the inclusions are estimated as 2.5–0.1 wt.% NaCl and 0.8–0.1 wt.% KCl, however, the presence of Fe and Mg chlorides in the composition of the inclusions is unlikely. Mg compounds are not typical for the studied mineral associations. $FeCl_2$ and $FeCl_3$ in water–salt systems would cause a metastable state, which also would involve incomplete crystallization of the cooled solution and, as a consequence, a decrease in the melting point of the eutectic [49,50], which was not observed in our studies.

Cryometric study of individual vapor inclusions and the gas component of water–salt inclusions did not reveal the presence of a dense gas phase. The cooling down to −190 °C did not result in any gases' liquefaction or crystallization. The absence of a dense gas phase is also confirmed by the study of fluid inclusions with Raman spectroscopy. Raman spectra of the gas phase of inclusions do not contain bands characteristic of $CO_2$, $N_2$, and $CH_4$ [51].

The pressure values were calculated for the concentration of solutions (wt.%) equivalent to NaCl. These values decrease from early generations of quartz to later ones and are in the range of 70–13 bar for the pyrite-quartz association.

### 4.3.2. Maletoyvayamite-Quartz Association

Two-phase inclusions in the early quartz of the maletoyvayamite-quartz association were homogenized in a temperature range from 255 to 245 °C. Ice is formed in cooled solutions of two-phase inclusions, which then is melted at temperatures ranging from −2.5 to −2 °C. The beginning of ice melting in cooled solutions occur in the range from −38 to −35 °C. Fluid inclusions in late quartz from veinlets were homogenized in a temperature range from 225 to 135 °C (Table 4).

The rate of ice melting in cooled inclusions increases sharply at temperatures above −23 °C, and lastly ice melts in a temperature range from −0.7 to −0.3 °C. The temperature ranges for the initial melting point of cooled solutions in the inclusions are close to the melting temperature of the eutectic of the water–salt systems $Na_2CO_3 + K_2CO_3 + H_2O$ and $K_2CO_3 + H_2O$: −37 °C and −36.4 °C, respectively. A quick acceleration of ice melting in cooled solutions at a temperature of −23 °C suggests the presence of NaCl and KCl solutions along with $Na_2CO_3$ and $K_2CO_3$ as part of the composition.

The water–salt inclusions of the ore-bearing minerals from the maletoyvayamite-quartz association are more saturated in salts in comparison with the inclusions from the pyrite-quartz association (Table 4). Salt concentrations were calculated by the method of Borisenko [41], reaching NaCl = 3.3 and 1.0, and KCl = 1.0 and 0.5 (wt.%) in early quartz and late quartz, respectively. These values decrease from early generations of quartz to later ones and are in the range of 39–4 bar for the maletoyvayamite-quartz association (Table 4, Figure 10).

### 5. Discussion

The results obtained from fluid inclusions microthermometry in vein quartz of the Maletoyvayam deposit (Gaching area) indicate that the quartz was formed in a wide range of temperatures from nearly 300 to 180 °C and even below. In the same way, the pressure also varies from 80 to 10 bar (average). At high temperatures (295–255 °C) and pressures (50–75 bar), pyrite is the main ore mineral (pyrite-quartz association) (Figure 11a), while maletoyvayamite, bismuthinite, Cu-sulfosalts, etc. occurred in a rather narrow range of temperatures and pressures (245–255 °C and 32–39 bar) (Figure 12).
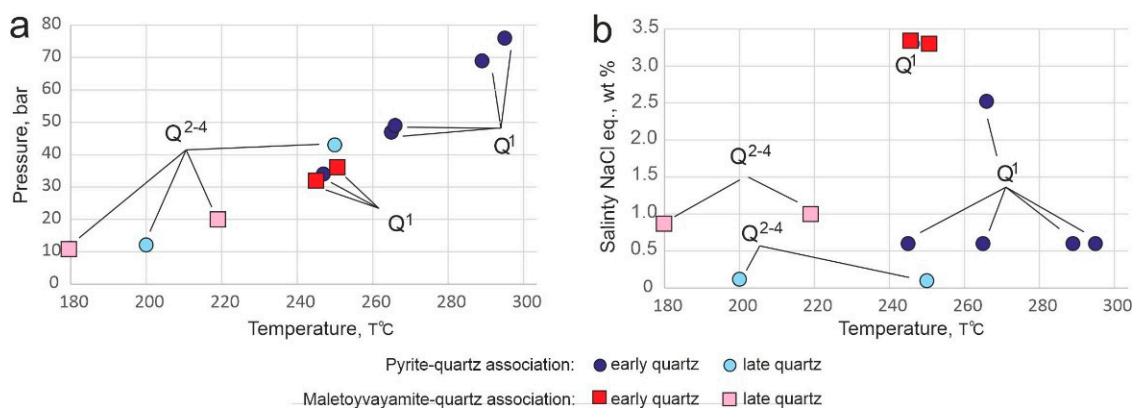


**Figure 11.** (**a**) Diagrams of pressure versus temperature and (**b**) salinity of NaCl eq. versus temperature on the basis of the microthermometry study of the different quartz generations.
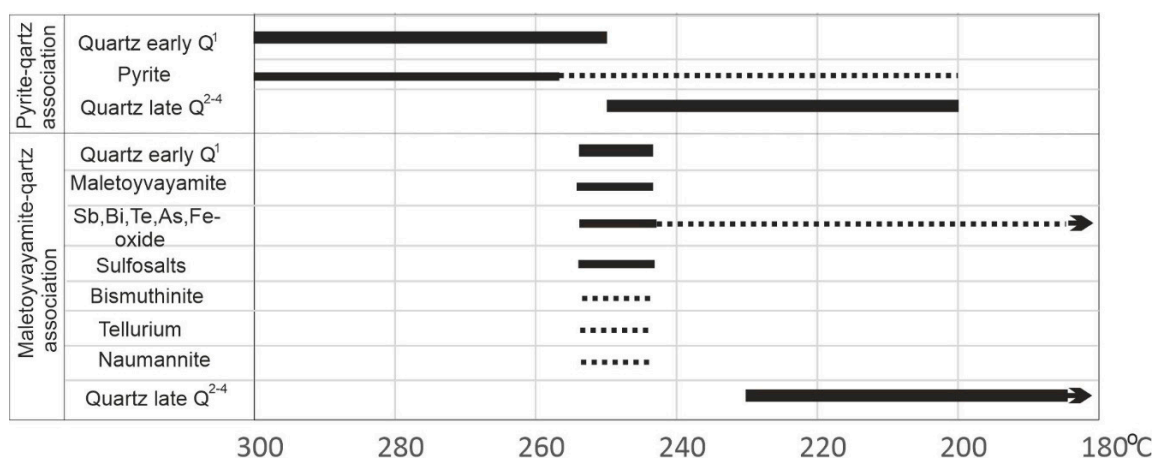
**Figure 12.** Paragenetic diagram showing the stages of mineral formation. The thick line – main mineral, line - less common mineral, dotted line – rare mineral.

Both of the diagrams in (Figure 11) display a gradual change between the mineral associations, moving from pyrite-quartz to maletoyvayamite-quartz; the late quartz generation of the first association coincides with the early quartz generation of the second association in P-T parameters (Figure 11a); however, they do differ in salt content (Figure 11b). For instance, the salinity percentage in fluid inclusions of the productive gold-bearing association (maletoyvayamite-quartz) is considerably bigger (3.3 versus 0.6).

Sulfosalts are an important indicator of mineral formation conditions in hydrothermal deposits of various types [52–54]. Enargite in particular is a formation conditions indicator of HS type epithermal deposits [2]. This mineral has been found in ores of well-known HS epithermal deposits: Goldfield (Nevada, USA), Red Mountain, Lake City II and Summitville (Colorado, USA), Julcani (Peru) [2,55,56] and others. It is also common among the sulfosalts described at Maletoyvayam [33], and, in particular, in the studied samples (Figure 5). Enargite-bearing epithermal deposits develop when fluid rapidly rises to higher levels of the earth's crust without interacting with groundwater. Then, its gradual cooling and partial neutralization due to its reaction with the host rocks leads to the formation of a pyrite–enargite association, including alunite and barite [57].

Earlier, we made the assumption that pyrite formation and maletoyvayamite are divergent in time based on the fact that they have never been encountered in equilibrium intergrowths [26]. Indeed, the microthermometry study on fluid inclusions in quartz confirmed this hypothesis: the most abundant dissemination of pyrite grains occur in the earliest generations of the fine-grained quartz aggregate (Figure 8a), with temperatures that correspond to a range of 295–245 °C, whereas the Au minerals, sulfosalts and other associated minerals of the main ore stage crystallized at 255–245 °C (Table 3, Figures 10 and 12). Moreover, pyrite crystallization precedes enargite in many HS-type epithermal deposits [58].

The fluid inclusions data for HS epithermal deposits (Table 5) indicate that ore deposition occurred mainly at temperatures similar to the LS and IS types. For example, the homogenization temperatures of primary inclusions in quartz from the Aginskoye deposit (LS type) were 230–280 °C, with the ore phase being in the range of 250–260 °C [59]. Similar temperature ranges have been established both for the LS type deposits (Rodnikovoye and Asachinskoye in South Kamchatka, Russia) [19,21,60] and in regard to the IS type deposit (Cheshmeh Hafez, Iran) [61], the homogenization temperatures of the primary inclusions are in the range of 140–280 °C with peaks at around 180–250 °C. This is also compatible with all HS type deposits, and with the obtained formation parameters of the Maletoyvayam deposit (Table 5).

The salinity of ore-forming solutions differs both between the deposit types (LS and HS) and even within the same type (Table 5). The salinity range can be strongly influenced on one hand by the

mixing with meteoric water (dilution), or, on the other hand, by boil-off (concentrating) [57,62]. Fluid inclusions with high salinity reflect the fluid history after crystallization of underlying magmas [63,64]. The strongly acidic hot fluids interaction with host rocks typically dissolve the surrounding rock, leaving only silica. Then, brines containing gold ascend from the magma and precipitate metals in the vuggy quartz forming the HS deposits. In general, the salinity of HS type deposits show a wide range of values. For example, the highest salinity values of HS type ore deposits range from 5 to 24 wt.% NaCl eq. for Julcani, Summitville and Goldfield [65,66] (Table 5). The ranges of 3–12 wt.% NaCl eq. are typical of the Kairagach and Shelekhovskoe [67,68]. However, data from fluid inclusions in quartz associated with the main gold stage from Red Mountain, Mt Carlton, Lepanto, Agan, Danchenkovskoe and Belaya Gora [27,69–72], including Maletoyvayam, indicate salinities of up to 4.5 wt.% NaCl eq. (Table 5).

**Table 5.** Crystallization conditions parameters for HS type epithermal deposits.

| District | Measured | | Selected Ore Representative | | References |
|---|---|---|---|---|---|
| | T °C | Salinity | T °C | Salinity | |
| Red Mountain, BC, Canada | 215–265 (?) | 1.6 | 240 | 1.6 | [69] |
| Summitville, CO | 231–276 (?) | 7–21 | | | [65] |
| Goldfield, NV | 150–325 (?) | 5–18 | | | [65,66] |
| Julcani, Peru | 161–275 (?) | 5–24 | | | [65] |
| Mt Carlton, NE Australia | 163–264 (57) | 0–1.6 | 222 | | [70] |
| Lepanto, Philippines | 166–285 | 0.2–4.5 | | | [71] |
| Kairagach, Uzbekistan | 120–300 | <12 | | | [67] |
| Agan, Russia | 88–184 (6) | 0.2–2.6 | 136 | | [27] |
| Danchenkovskoe, Russia | 297–336 | 1–4 | | | [72] |
| Belaya Gora, Russia | ≈100 | <1 | | | [68] |
| Shelekhovskoe, Russia | 180–250 | 3–8 | | | |
| Maletoyvayam * Russia | 295–245 (23) | 0.9–3.3 | 270 | 2 | This study |
| Maletoyvayam ** | 255–245(6) | 4.3 | 250 | 4.3 | This study |
| Maletoyvayam *** | 228–135(9) | 1.3 | 180 | 1.3 | This study |

Note. *—pyrite-quartz association (early $Q^1$); **—maletoyvayamite-quartz association (early $Q^1$); ***—maletoyvayamite-quartz association (later $Q^{2-4}$). Salinity in wt. % NaCl eq. Selected Temperature and Salinity related to the productive stage.

The HS mineralization associated with the dilute to moderately saline solutions (<5 to ~10 wt.% NaCl eq.) occur at temperatures between 180 and 320 °C [71]. The hotter and more saline fluid inclusions occur in rocks of deep horizons closer to the magma fluid source [14,73]. The reduction in the sulfidation state of fluids due to interaction with wallrocks can change HS fluids to IS ones, as confirmed by paragenetic transitions from HS to IS mineralization [74]. In the IS-type epithermal deposits, salinity ranges vary widely and reaches high values, for example, 4.7–18 wt.% NaCl eq. at the Cheshmeh Hafez field [61]. While the salinity in inclusions from LS-type deposits of the Aginskoye deposit of the Central Kamchatka volcanic belt is no more than 2 wt.% NaCl equiv. [59], as in the Juliet field (LS-type), at the Okhotsk-Chukotka volcanic belt, the salinity of the inclusions is about 1.2–5.6 wt.% NaCl eq. [75]. In this respect, it is clear that the salinity of fluid inclusions is not intimately related to the type of deposit, but more dependent on the conditions of ore deposition.

Based on the formation model for HS epithermal deposits [4,39,64,76,77], it can be assumed that gold–copper–porphyry mineralization may be found at deeper horizons in the Maletoyvayam area since the models for epithermal deposits form in a relatively near-surface magmatic-hydrothermal environment associated with volcanic rocks that overlie cogenetic intrusive rocks.

## 6. Conclusions

Two mineral associations were indentified during the study of quartz mineralization at the Maletoyvayam Au-deposit: the earlier pyrite-quartz and the Au-bearing maletoyvayamite-quartz associations. Each of them contains different generations of quartz, but only the early quartz generations

in each of the mentioned associations include either pyrite (pyrite-quartz association) or sulfosalts with gold compounds and other rare associating minerals (maletoyvayamite-quartz association). Maletoyvayamite is the main Au mineral of the maletoyvayamite-quartz association, which has never been reported in any other epithermal gold deposit in the world. It was particularly identified in samples having high Au concentrations, and occurs in the marginal parts of sulfosalts, intergrown with complex oxides of chalcogenides and native tellurium, and also as individual inclusions in quartz.

The following features and physicochemical conditions on the formation of a productive ore association were identified based on the fluid inclusions study (Figures 11 and 12):

The composition of primary fluid inclusions in the quartz is represented by the dominant NaCl and KCl, as well as $Na_2CO_3$ and $K_2CO_3$. The total percentage of salinity varies from 4.3 wt.%. in the early quartz from the maletoyvayamite-quartz association to 0.2 in late quartz from the pyrite-quartz association. The temperature of fluids varied from 290 to 135 °C, decreasing during the crystallization of the later generations of quartz (Figure 11). The calculated pressure of the fluid varies from 79 to 4 bar, and most likely corresponds to hydrostatic fluid. The fluids that formed the maletoyvayamite-quartz association differ from those forming the pyrite-quartz association with lower temperatures (255–135 °C), and increased salt concentration (4.3 wt.%). The increase in the total concentration of salts in the hydrothermal solutions that formed the maletoyvayamite-quartz association is due to the boiling of fluids. All parameters before presented and discussed agree in all respects with other HS-type epithermal deposits around the world; however, they do not provide further evidence of the particularities in ore mineral composition of the Maletoyvayam deposit, which is as yet the only known occurrence of the HS type on the Central Kamchatka Volcanic Belt.

## References

1. Lindgren, W. *Mineral. Deposits*; McGraw-Hill Book Company, Inc.: New York, NY, USA; London, UK, 1933; p. 930.

2. Heald, P.; Hayba, D.O.; Foley, N.K. Comparative anatomy of volcanic-hosted epithermal deposits: Acid-sulfate and adularia-sericite types. *Econ. Geol.* **1987**, *82*, 1–26. [CrossRef]

3. Taylor, B.E. Epithermal gold deposits. In *Mineral. Deposits of Canada: A Synthesis of Major Deposit-Types, District Metallogeny, the Evolution of Geological Provinces, and Exploration Methods*; Goodfellow, W.D., Ed.; Mineral Deposits Division, Special Publication; Geological Association of Canada: Saint John, NL, Canada, 2007; Volume 5, pp. 113–139.

4. Hedenquist, J.W.; Arribas, A.; Gonzalez-Urien, E. Exploration for epithermal gold deposits. *Rev. Econ. Geol.* **2000**, *13*, 245–277.

5. Hedenquist, J.W. Mineralization associated with volcanic-related hydrothermal systems in the Circum-Pacific basin. In *Transactions of the Fourth Circum Pacific Conference on Energy and Mineral Resources Conference, Singapore*; American Association of Petroleum Geologists: Tulsa, OK, USA, 1987; pp. 513–524.

6.    Ashley, R.P. Occurrence model for enargite-gold deposits. In *U.S. Geological Survey Open-File Report 82-795*; U.S. Department of the Interior, Geological Survey USA: Reston, VA, USA, 1982; pp. 144–147.

7.    Bethke, P.M. Controls on base- and precious-metal mineralization in deeper epithermal environments. In *US Geological Survey Open-File Report 84–890*; U.S. Dept. of the Interior, Geological Survey USA: Reston, VA, USA, 1984; 39 p.

8.    Ransome, F.L. The association of alunite with gold in the Goldfield district, Nevada. *Econ. Geol.* **1907**, *2*, 801–803. [CrossRef]

9.    Bonham, H.F. Three major types of epithermal precious metal deposits. *Geol. Soc. Am. Abstr. Programs* **1984**, *16*, 449.

10.   Bonham, H.F., Jr. Models for volcanic-hosted epithermal precious metal deposits: A review. In *Proceedings Symposium 5th, Volcanism, Hydrothermal Systems and Related Mineralisation*; International Volcanological Congress: Auckland, New Zealand, 1986; pp. 13–17.

11.   Berger, B.R. Descriptive model of low-sulfide Au-quartz veins. In *Mineral deposit models, US Geological Survey Bulletin*; United States Government Printing Office: Washington, DC, USA, 1992; p. 239.

12.   Berger, B.R.; Henley, R.W. Advances in the understanding of epithermal gold-silver deposits, with special reference to the western United States. *Econ. Geol. Monogr.* **1989**, *6*, 405–423.

13.   Henley, R.W.; Ellis, A.J. Geothermal systems ancient and modern: A geochemical review. *Earth Sci. Rev.* **1983**, *19*, 1–50. [CrossRef]

14.   Arribas, A., Jr. Characteristics of high-sulfidation epithermal deposits, and their relation to magmatic fluid. *Mineral. Assoc. Can. Short Course* **1995**, *23*, 419–454.

15.   Kubota, Y. Temporal and spatial relationship and significance of island arc junctions on Late Cenozoic gold deposits in the Japanese Islands. *Res. Geol.* **1994**, *44*, 17–24.

16.   Okrugin, V.; Kokarev, S.; Okrugina, A.; Chubarov, V.; Shuvalov, R. An unusual example of the interaction of modern hydrothermal system with Au-Ag veins (Southern Kamchatka). *Miner. Mag.* **1994**, *58A*, 669–670. [CrossRef]

17.   Khanchuk, A.I.; Ivanov, V.V. Meso-Cenozoic geodynamic settings and gold mineralization of the Russian Far East. *Russ. Geol. Geophys.* **1999**, *40*, 1607–1617.

18.   Konstantinov, M.M.; Vargunina, N.P.; Kosovets, T.N.; Struzhkov, S.F.; Syngaevskii, E.D.; Shishakova, L.N. *Gold-Silver Deposits. Series: Models of Noble-and Nonferrous-Metal Deposits*; TsNIGRI: Moscow, Russia, 2000; 239p. (In Russian)

19.   Borovikov, A.A.; Lapukhov, A.S.; Borisenko, A.S.; Seryotkin, Y.V. The Asachinskoe epithermal Au-Ag deposit in southern Kamchatka: Physicochemical conditions of formation. *Russ. Geol. Geophys.* **2009**, *50*, 693–702. [CrossRef]

20.   Takahashi, R.; Matsueda, H.; Okrugin, V.M. Hydrothermal gold mineralization at the Rodnikovoe deposit in South Kamchatka, Russia. *Res. Geol.* **2002**, *52*, 359–369. [CrossRef]

21.   Takahashi, R.; Matsueda, H.; Okrugin, V.M.; Ono, S. Epithermal gold-silver mineralization of the Asachinskoe deposit in South Kamchatka, Russia. *Resour. Geol.* **2007**, *57*, 354–373. [CrossRef]

22.   Okrugin, V.M.; Shishkanova, K.O.; Yablokova, D.A. About ores of Amethystovoe deposits (Kamchatka). *Mt. Bull. Kamchatka* **2015**, *3-4*, 33–34. (In Russian)

23.   Andreeva, E.D.; Matsueda, H.; Okrugin, V.M.; Takahashi, R.; Ono, S. Au–Ag–Te mineralization of the low-sulfidation epithermal Aginskoe deposit, Central Kamchatka, Russia. *Res. Geol.* **2013**, *63*, 337–349. [CrossRef]

24.   Golyakov, V.I. *Geological Map of the USSR Scale 1: 200 000*; Pogozhev, A.G., Ed.; Series Koryak; Sheets P-5 8-XXXIII, O-58-III.; VSEGEI Cartographic Factory: St. Peterburg, Russia, 1980. (In Russian)

25.   Melkomukov, B.H.; Razumny, A.V.; Litvinov, A.P.; Lopatin, W.B. New highly promising gold objects of Koryakiya. *Min. Bull. Kamchatka* **2010**, *14*, 70–74. (In Russian)

26.   Tolstykh, N.; Vymazalova, A.; Tuhy, M.; Shapovalova, M. Conditions of formation of Au-Se-Te mineralization in the Gaching ore occurrence (Maletoivayam ore field), Kamchatka, Russia. *Min. Mag.* **2018**, *82*, 649–674. [CrossRef]

27.   Volkov, A.V.; Sidorov, A.A.; Chizhova, I.A.; Alekseev, V.Y.; Savva, N.E.; Kolova, E.E. The Agan epithermal gold-silver deposit and prospects for the discovery of high-sulfidation mineralization in Northeast Russia. *Geol. Ore Depos.* **2015**, *57*, 21–41. [CrossRef]

28. Goryachev, N.A.; Volkov, A.V.; Sidorov, A.A.; Gamyanin, G.N.; Savva, N.Y.; Okrugin, V.M. Au-Ag-mineralization of volcanogenic belts of the northeast. Asia. *Lithosphere* **2010**, *3*, 36–50. (In Russian)

29. Palyanova, G.A. Gold and Silver Minerals in Sulfide Ore. *Geol. Ore Depos.* **2020**, *62*, 383–406. [CrossRef]

30. Tolstykh, N.D. Gold ore mineralization of the Maletoyvayam ore occurrence. In *Materials of the Anniversary Congress of the Russian Mineralogical Society "200 Years of RMO"*; LLC Publishing House LEMA: St. Peterburg, Russia, 2017; Volume 2, pp. 339–341.

31. Tolstykh, N.; Palyanova, G.; Bobrova, O.; Sidorov, E. Mustard gold of the Gaching ore occurrence (Maletoyvayam deposit, Kamchatka, Russia). *Minerals* **2019**, *9*, 489. [CrossRef]

32. Tolstykh, N.D.; Tuhý, M.; Vymazalová, A.; Plášil, J.; Laufek, F.; Kasatkin, A.V.; Nestola, F.; Bobrova, O.V. Maletoyvayamite, $Au_3Se_4Te_6$, a new mineral from Maletoyvayam deposit, Kamchatka peninsula, Russia. *Min. Mag.* **2020**, *84*, 117–123. [CrossRef]

33. Shapovalova, M.; Tolstykh, N.; Bobrova, O. Chemical composition and varieties of sulfosalts from gold mineralization in the Gaching ore occurrence (Maletoyvayam ore field). *IOP Conf. Ser. Earth Environ. Sci.* **2019**, *319*, 012019. [CrossRef]

34. Palyanova, G.A.; Tolstykh, N.D.; Zinina, V.Y.; Koh, K.A.; Seretkin, Y.V.; Bortnikov, N.S. Synthetic gold chalcogenides in the Au-Te-Se-S system and their natural analogs. *Dokl. Earth Sci.* **2019**, *487*, 929–934. [CrossRef]

35. Palyanova, G.; Mikhlin, Y.; Zinina, V.; Kokh, K.; Seryotkin, Y.; Zhuravkova, T. New gold chalcogenides in the Au-Te-Se-S system. *J. Phys. Chem. Solids.* **2020**, *138*, 109276. [CrossRef]

36. Vlasov, G.M. *Volcanic Sulfur Deposits and Some Problems of Hydrothermal ore Formation*; Nauka: Moscow, Russia, 1971. (In Russian)

37. Stefanov, Y.M.; Schiroky, B.I. *Metallogeny of the Upper Structural Floor of Kamchatka*; Science: Moscow, Russia, 1980. (In Russian)

38. Melkomukov, V.N.; Amelin, S.A.; Razumny, A.V.; Kudrin, A.S. *State Geological Map of the Russian Federation on a Scale of 1: 200 00*; Lopatin, V.B., Ed.; Series Olyutorsky; Sheet P-58-XXXIII, O-58-III.; VSEGEI Cartographic Factory: St. Petersburg, Russia, 2010. (In Russian)

39. White, N.C.; Hedenquist, J.W. Epithermal gold deposits: Styles, characteristics and exploration. *Publ. SEG Newsl.* **1995**, *23*, 9–13.

40. Hedenquist, J.W.; Arribas, R.A. Epithermal ore deposits: First-order features relevant to exploration and assessment. In Proceedings of the 14th SGA Biennial Meeting, Québec City, QC, Canada, 20–23 August 2017; Volume 1, pp. 47–50.

41. Borisenko, A.S. Analysis of the salt composition of solutions of gas-liquid inclusions in minerals by cryometry. In *The Use of Methods of Thermobarogeochemistry in the Search and Study of Ore Deposits*; Nedra: Moscow, Russia, 1982; pp. 37–47. (In Russian)

42. Bodnar, R.J.; Vityk, M.O. Interpretation of microthermometric data for $NaCl-H_2O$ fluid inclusions. In *Fluid Inclusions in Minerals: Methods and Applications*; Virginia Polytechnic Institute State University: Blacksburg, VA, USA, 1994; pp. 117–131.

43. Bakker, R.J. AqSo_NaCl: Computer program to calculate p-T-V-x properties in the H2O-NaCl fluid system applied to fluid inclusion research and pore fluid calculation. *Comput. Geosci.* **2018**, *115*, 122–133. [CrossRef]

44. Bakker, R.J. Fluids: New software package to handle microthermometric data and to calculate isochors. *Mem. Geol. Soc.* **2001**, 23–25.

45. Brown, P.E. FLICOR: A microcomputer program for the reduction and investigation of fluid-inclusion data. *Am. Min.* **1989**, *74*, 1390–1393.

46. Voudouris, P.; Melfos, V.; Spry, P.G.; Moritz, R.; Papavassiliou, K.; Falalakis, G. Mineralogy and geochemical environment of formation of the Perama Hill high-sulfidation epithermal Au-Ag-Te-Se deposit, Petrota Graben, NE Greece. *Min. Petrol.* **2011**, *103*, 79–100. [CrossRef]

47. Roedder, E. Fluid inclusions. In *Reviews in Mineralogy*; Mineralogical Society of America: Washington, DC, USA, 1984; Volume 12, pp. 79–108.

48. Ermakov, N.P. *Geochemical Systems of Inclusions in Minerals*; Nedra: Moscow, Russia, 1972. (In Russian)

49. Lecumberri-Sanchez, P.; Steele-MacInnis, M.; Bodnar, R.J. Synthetic fluid inclusions XIX. Experimental determination of the vapor-saturated liquidus of the system $H_2O–NaCl–FeCl_2$. *Geochim. Cosmochim. Acta* **2015**, *148*, 34–49. [CrossRef]

50. Borovikov, A.A.; Gushchina, L.V.; Borisenko, A.S. Determination of iron (II, III) and zinc chlorides in solutions of fluid inclusions during cryometric studies. *Geochemistry* **2002**, *1*, 70–79. (In Russian)

51. Frezzotti, M.L.; Tecce, F.; Casagli, A. Raman spectroscopy for fluid inclusion analysis. *J. Geochem Explor.* **2012**, *112*, 1–20. [CrossRef]

52. Spiridonov, E.M. Typomorphic specific features of Fahlore from some plutonogenic, volcanogenic, and telethermal gold deposits. *Geol. Rudn. Mestorozhd.* **1987**, *29*, 83–92. (In Russian)

53. Repstock, A.; Voudouris, P.; Kolitsch, U. New occurrences of watanabeite, colusite, "arsenosulvanite" and Cu-excess tetrahedrite-tennantite at the Pefka high-sulfidation epithermal deposit, northeastern Greece. *Neues Jahrb. Fur Mineral. Abh. J. Mineral. Geochem.* **2015**, *192*, 135–149. [CrossRef]

54. Kovalenker, V.A.; Bortnikov, N.S. Chemical composition and mineral associations of sulphosalts in the precious metal deposits from different geological environment. *Geol. Carpathica* **1985**, *36*, 283–291.

55. Buchanan, L.J. Precious metal deposits associated with volcanic environments in the southwest. *Ariz. Geol. Soc. Dig.* **1981**, *14*, 237–262.

56. Hayba, D.O.; Bethke, P.M.; Heald, P.; Foley, N.K. Geologic, mineralogic and geochemical characteristics of volcanic-hosted epithermal precious metal deposits. *Rev. Econ. Geol.* **1985**, *2*, 129–167.

57. Corbett, G. Epithermal Au-Ag Deposit Types—Implications for Exploration. 2005. Available online: https://www.researchgate.net/publication/237489786 (accessed on 30 August 2014).

58. Jannas, R.; Bowers, T.S.; Petersen, U.; Beane, E. High-Sulfidation Deposit Types in the El Indio District, Chile. In *Geology and Ore Deposits of the Central Andes*; Skinner, B.J., Ed.; Society Economic Geologists Special Publication: Littleton, CO, USA, 1999; Volume 7, pp. 27–59.

59. Okrugin, V.M.; Andreeva, E.D.; Yablokova, D.A.; Okrugina, A.M.; Chubarov, V.M.; Ananiev, V.V. The new data on the ores of the Aginskoye gold-telluride deposit (Central Kamchatka). In *"Volcanism and Its Associated Processes" Conference*; Petropavlovsk-Kamchatsky: Kamchatka Krai, Russia, 2014; pp. 335–341. (In Russian)

60. Takahashi, R.; Matsueda, H.; Okrugin, V. Epithermal gold and silver mineralization at the Rodnikovoe deposit related to the hydrothermal activity in the Mutnovsko-Asachinskaya geothermal area, Southern Kamchatka, Russia. In Proceedings of the International Symposium on Gold and Hydrothermal Systems, Fukuoka, Japan, 4 November 2001; pp. 51–57.

61. Mehrabi, B.; Siani, M.G. Intermediate sulfidation epithermal Pb-Zn-Cu (±Ag-Au) mineralization at Cheshmeh Hafez deposit, Semnan Province. *J. Geol. Soc. India* **2012**, *80*, 563–578. [CrossRef]

62. Hedenquist, J.W.; Henley, R.W. Hydrothermal eruptions in the Waiotapu geothermal system, New Zealand: Their origin, associated breccias, and relation to precious metal mineralization. *Econ. Geol.* **1985**, *80*, 1640–1668. [CrossRef]

63. Hedenquist, J.W.; Arribas, A.; Reynolds, T.J. Evolution of an intrusion-centered hydrothermal system: Far Southeast-Lepanto porphyry andepithermal Cu-Au deposits, Philippines. *Econ. Geol.* **1998**, *93*, 373–404. [CrossRef]

64. Heinrich, C.A.; Dreisner, T.; Steffánson, A.; Seward, T.M. Magmatic vapor contraction and the transport of gold from the porphyry environment to epithermal ore deposits. *Geology* **2004**, *32*, 761–764. [CrossRef]

65. Bruha, D.I.; Noble, D.C. Hypogenequartz-alunite±pyrite alteration formed by moderately saline, ascendant hydrothermal solutions. *Geol. Soc. Am. Abstr. Programs* **1983**, *15*, 325.

66. Jensen, M.L.; Ashley, R.P.; Albers, J.P. Primary and secondary sulfates at Goldfield, Nevada. *Econ. Geol.* **1971**, *66*, 618–626. [CrossRef]

67. Kovalenker, V.A.; Plotinskaya, O.Y.; Prokofev, V.Y.; Gertman, Y.L.; Koneev, R.I.; Pomortsev, V.V. Mineralogy, geochemistry, and genesis of gold-sulfide-selenide-telluride ores from the Kairagach deposit (Uzbekistan). *Geol. Ore Depos.* **2003**, *45*, 171–200.

68. Mishin, L.F.; Berdnikov, N.V. Nature of high-alumina secondary quartzite by data of thermobarogeochemistry and isotopic analysis of oxygen and hydrogen. *Russ. J. Pac. Geol.* **2001**, *20*, 123–139. (In Russian)

69. Nash, J.T. Fluid inclusion studies of vein, pipe, and replacement deposits, northwestern San Juan Mountains, Colorado. *Econ. Geol.* **1975**, *70*, 1448–1462. [CrossRef]

70. Sahlstrom, F. The Mt Carlton High-Sulfidation Epithermal Deposit, NE Australia: Geologic Character, Genesis and Implications for Exploration. PhD. Thesis, James Cook University, Singapore, 2018.

71. Mancano, D.P.; Campbell, A.R. Microthermometry of enargite-hosted fluid inclusions from the Lepanto, Philippines, high-sulfidation Cu-Au deposit. *Geochim. Cosmochim. Acta* **1995**, *59*, 3909–3916. [CrossRef]

72. Lapukhov, A.S.; Borovikov, A.A.; Guzman, B.V.; Miroshnichenko, L.V.; Rasvorotneva, L.I. Hieratite in hydrothermally altered volcanic rocks of Danchenkovskoye deposit (the Urup Island). *Zap. RMO* **2012**, *141*, 52–59. (In Russian)

73. Arribas, A., Jr.; Cunningham, C.G.; Rytuba, J.J.; Rye, R.O.; Kelly, W.C.; Podwysocki, M.H.; McKee, E.H.; Tosdal, R.M. Geology, geochronology, fluid inclusions, and isotope geochemistry of the Rodalquilar gold-alunite deposit, Spain. *Econ. Geol.* **1995**, *90*, 795–822. [CrossRef]

74. Sillitoe, R.H.; Hedenquist, J.W. Linkages between volcanotectonic settings, ore-fluid compositions, and epithermal precious metal deposits. In *Volcanic, Geothermal, and Ore-Forming Fluids: Rulers and Witnesses of Processes within the Earth*; Simmons, S.F., Graham, I.J., Eds.; Society Economic Geologists Special Publication: Johnson Printing, Littleton, CO, USA, 2003; Volume 10, pp. 315–343.

75. Prokof′ev, V.Y.; Ali, A.A.; Volkov, A.V.; Savva, N.E.; Kolova, E.E.; Sidorov, A.A. geochemical peculiarities of ore forming fluidof the juliette Au–Ag epithermal deposit (Northeastern Russia). *Dokl. Earth Sci.* **2015**, *460*, 87–91. [CrossRef]

76. Cooke, D.R.; Simmons, S.F. Characteristics and genesis of epithermal gold deposits. *Rev. Econ. Geol.* **2000**, *13*, 221–244.

77. Sillitoe, R.H. Porphyry copper systems. *Econ. Geol.* **2010**, *105*, 3–41. [CrossRef]

**Publisher's Note:** MDPI stays neutral with regard to jurisdictional claims in published maps and institutional affiliations.